Comparative analysis of energy performance of squirrel cage induction motor, line-start synchronous reluctance and permanent magnet motors employing the same stator design

Wieslaw Lyskawinski

Poznan University of Technology
Institute of Electrical Engineering and Electronics
Piotrowo 3A str., 60-965 Poznan, Poland
e-mail: wieslaw.lyskawinski@put.poznan.pl

Abstract: The paper presents research on the development of a line-start synchronous reluctance motor (LSSynRM) and line-start permanent magnet synchronous motor (LSPMSM) based on components of a mass-produced three-phase low-power squirrel cage induction motor (IM). The aim of the research was to modify the squirrel cage rotor structure for which the best functional parameters characterizing the steady state of the LSSynRM and LSPMSM were obtained, while meeting the additional requirements for asynchronous start-up. Field-circuit models of the LSSynRM and LSPMSM have been developed in the professional finite element method (FEM) package, MagNet, and applied in the design and optimization calculations of the considered machines. Experimental testing on the designed LSSynRM and LSPMSM prototypes were carried out. The obtained results were compared with the performance of the reference IM. The conclusions resulting from the comparative analysis of these three motors are given and proposals for further work are discussed.

Key words: efficiency, experimental testing, FE models of LSSynRM, IM, LSMPSM, power factor, simulation calculations

1. Introduction

The AC motors, especially synchronous, are an important element of industrial drives and household appliances. They are mainly used where constant speed or synchronization of the rotation of many non-mechanically connected axes is required. The need to develop low-cost and

reliable low-power electric propulsion systems, operating at constant speed, prompted the author to undertake research on an LSPMSM and LSSynRM. Thanks to a rotor cage winding these motors do not require expensive power electronics for start-up and speed stabilization, which also increases drive reliability. Asynchronous torque generated by the rotor squirrel cage is used for start-up. The disadvantages of asynchronous start-up are high values of the inrush current during the direct line-start process and risk to fail synchronization for loads of high inertia [1, 2]. For these reasons, most of the line-start motors have relatively low power, however a high power LSPMSM has been recently reported among others by [3]. Designed line-start synchronous motors should meet the requirements for steady-state operation parameters and requirements related to asynchronous operation, regarding a minimum of: start-up torque, breakdown torque and pull-in torque falling into synchronism [2, 4–7].

In drive systems operating at constant rotational speed it is advantageous to use an LSPMSM instead of a classical squirrel cage IM supplied by the frequency converters. The LSPMSM offers higher power density and better functional parameters characterizing steady state operation in comparison to the IM. On the other hand, the cost of producing permanent magnet machines is greater than the cost of producing the LSSynRM. In addition, the magnets in the LSPMSM machine are exposed to irreversible demagnetization when the motor is operating at elevated ambient temperature and as a result of the armature reaction field occurring during fault conditions [8]. Intensive researches on the process of irreversible demagnetization of magnets held in many science centres [9–12].

As discussed in [13] the LSPMSMs as well as LSSynRMs are competitive with respect to induction motors used in low-power drives operating at constant rotational speed. As the motor frame sizes are standardized, the easiest and cheapest way to design the LSSynRM or LSPMSM is to use the stator core of the IM and modify the squirrel cage rotor to obtain non silent poles or insert the magnets into the rotor structure. The results of such modifications are fully functional LSSynRMs or LSPMSMs. However, it should be noticed that the rotors of LSPMSMs are magnetically and electrically heterogeneous in respect to magnetic flux excited by the stator winding. These asymmetries are the source of the so-called Görges effect, associated with generating a counter-rotating component of the magnetic field during the motor start-up. If the rotor magnetic and electrical circuits are incorrectly designed, too much of the counter-rotating field component is created and the electromagnetic torque generated by it can prevent the motor start-up. These motors have a slightly higher no-load current, lower efficiency, rated torque and power factor than the IMs used for their construction.

Rotors of the LSSynRM are characterized by intentionally introduced magnetic asymmetry achieved by placing magnetic flux barriers into the rotor magnetic circuit. These barriers are created by cutting holes in the rotor sheets in such a way that the remaining ferromagnetic material forms a magnetic flux path for high magnetic permeance [14–16]. The number of flux barriers depends on the machine structure and usually is one to eight per pole. Usually, a greater number of barriers per pole results in a greater ratio of magnetic permeance in the d-axis (machine poles) to permeance in the q-axis. The greater is this ratio the better functional parameters of the SynRM are achieved [17, 18].

Due to the presence of the magnetic flux source in the rotor, the LSPMSMs are characterized by much better energy performance, particularly higher torque density and efficiency. However, very high values of the inrush currents can flow in the stator winding during start-up (even several

times greater than the rated current). The value of the inrush currents and start-up time depend on the cage resistance and structure of the magnetic circuit as well as the inertia and the load torque value [1, 19]. The armature reaction field generated at start-up can lead to partial demagnetization of magnets. As a consequence, this may reduce the electromagnetic torque generated by the motor [20]. It is therefore important to correctly design and optimize the magnetic circuit of these machines [21, 22] to develop their new structures [3, 23–25] in order to obtain the best energy performance.

The development of low power LSSynRMs and LSPMSMs is also stimulated by recent achievements in research on new magnetic materials and magnetic core production technology [26]. Great hopes are associated with the use of cheap, non-waste production of cores from magnetic powder materials. The advantage of the core forming technology by magnetic powder pressing is obtaining a ready core in one press cycle and no need to assemble the core from steel sheets or to perform any additional mechanical treatment [27, 28].

The paper attempts to develop a low-cost LSPMSM and LSSynRM based on components of a mass-produced general-purpose three-phase IM. In order to avoid the necessity to fabricate a new rotor, the assumption was to design the LSPMSM and LSSynRM by modifications of the structure of IM's rotors. The introduced modifications tend to achieve the best functional parameters characterizing the steady state operation conditions of a synchronous motor, while meeting the requirements regarding asynchronous start-up at rated load.

Due to the non-linearity of the magnetic circuit, induced eddy currents and the complexity of electromagnetic phenomena in the considered motors as well as the requirement of high reliability of calculations, the field-circuit approach and the finite element method were used to analyze the operating states and to design magnetic circuits of the considered motors. The numerical field-circuit models of an IM, LSSynRM and LSPMSM were developed in a professional FEM package, MagNet. The measurements of the performance of the designed and built prototypes of the LSSynRM and LSPMSM were carried out and compared with the results of tests of the IM. Particular attention was paid to parameters of energy conversion quality, i.e. power factor and efficiency.

2. Numerical models and optimization of motors

Due to high reliability of the results, the finite element method (FEM) is one of the most commonly used approaches in the design and optimization process of electrical machines [29–31]. Conducting precise simulations of the machine performance reduces the cost and time to build and test motors prototypes. In the applied FEM package the vector magnetic potential A and the scalar electrical potential V formulation is used to develop a two-dimensional numerical model of the electromagnetic field distribution in the studied machines. In the applied method of the vector of magnetic flux density, B is expressed by the magnetic vector potential A:

$$B = \nabla \times A \,. \tag{1}$$

The magnetic field intensity vector H takes the form:

$$H = \mu^{-1} \nabla \times A \,, \tag{2}$$

where μ is the magnetic permeability of the domain.

The distribution of the electric field is described by the scalar electric potential V. The electric field strength vector E can be expressed by the sum of the field strength vector $E_s = \nabla V$ associated with external sources and the field strength vector $E_i = \partial A / \partial t$ induced by the magnetic field changes. After considering that for the current density vector J:

$$\nabla \cdot J = 0, \tag{3}$$

$$J = \sigma E, \tag{4}$$

the following equation is obtained:

$$\nabla \cdot [\sigma \, (\partial A / \partial t + \nabla V)] = 0, \tag{5}$$

where σ is the conductivity of the domain.

When the studied domain consists of permanent magnets, the additional component current density vector J_m representing the magnetization H_m of the permanent magnet is introduced as:

$$J_m = \nabla \times H_m, \tag{6}$$

where $B = \mu_0 \, (H + H_m)$ and μ_0 is the magnetic permeability of the vacuum.

On the basis of the above equations, taking into account Amperes' law, the electromagnetic field distribution can be determined by:

$$\nabla \left(\mu^{-1} \nabla \times A \right) = -\sigma \, (\partial A / \partial t + \nabla V) - \nabla \times H_m \,. \tag{7}$$

A two-dimensional numerical model of a three-phase four-pole induction motor of the Sh71-4A type with a rated power of 250 W and a rated speed of $n_N = 1390$ rpm was developed in the MagNet environment. It was taken into account that the stator and rotor cores were made of the M600 type electrical steel sheets. The machine has 24 slots in the stator and 18 slots in the rotor. The squirrel cage is made of aluminium. The stator winding is wound with a copper wire of 0.4 mm in diameter. The number of series connected conductors in a coil of the stator phase winding is 860. The motor cross-section and the applied FE mesh of the IM model are shown in Figs. 1(a) and (b), respectively. The mesh of the air gap between the stator and the rotor has been manually refined (Fig. 1(b)). The area under consideration has been discretized into over 100 000 elements and over 50 000 nodes. The remeshing method was used to map the rotor motion.

The rotor winding and the stator winding, together with the power supply, are modeled as electrical circuits (Fig. 2). Each rotor bar was represented by a separate coil with the resistance R_b and inductance L_b. The performed studies on the influence of the resistance and inductance of the end rings of the cage winding showed negligible importance of the results obtained in the analyzed motor operation modes. For this reason, the cage bars were shortened to simplify the model. The stator phase windings of the resistance R_s, leakage inductance L_{rs} and inductance L_{fem} (calculated by the field model) were supplied with the alternating voltages V_1, V_2, V_3, forming a three-phase balanced system.

In order to validate the model and confirm the reliability of the obtained results, the simulations of the motor performance have been carried out and the achieved results were compared with the results of experimental tests. The transient and steady state operation modes of the motor were

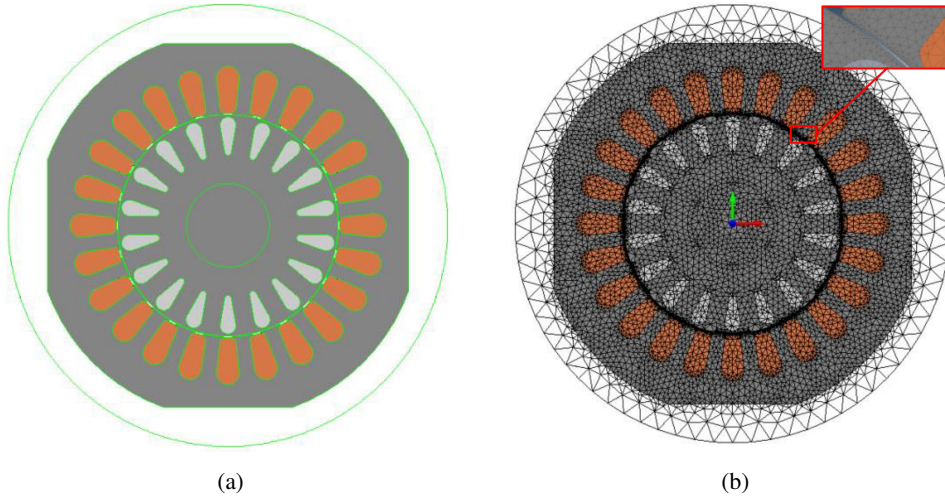(a)   (b)

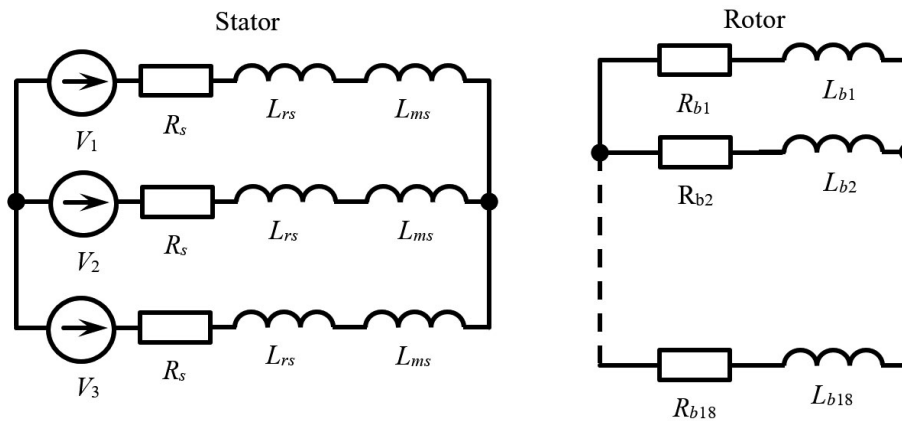Fig. 1. Cross-section of IM (a) and the grid discretization developed in IM model of MagNet (b)

Fig. 2. Connection diagram of the windings implemented in the developed model

analyzed. The paper contains only selected results of calculations concerning the analysis of the start-up process of a motor loaded with 1.73 Nm of rated torque. The resulting waveforms of stator phase currents, rotor speed during the start-up process and magnetic field distribution at steady-state operation are shown in Figs. 3 and 4, respectively. Satisfactory concordance between the simulation and experimental results – especially phase currents and rotor speed - was obtained. The presented results confirm the usefulness of the developed model for the analysis of an IM and indicate the desirability of using the formulated numerical model in the design calculations of LSSynRMs and LSPMSMs.

The LSSynRM and LSPMSM models differ from the IM model only in the rotor structure. Two variants (S1 and S2) of the LSSynRM rotor structures shown in Fig. 5(a) and 4(b) were
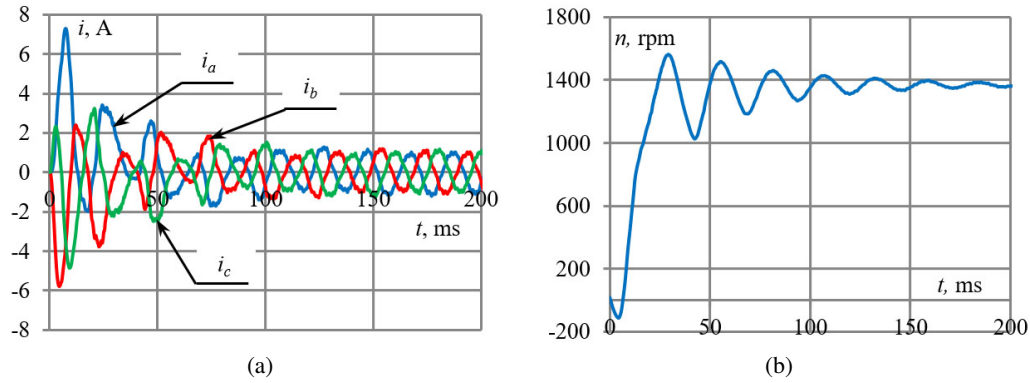
(a)

(b)

Fig. 3. Waveforms of current in stator windings (a) and rotational speed (b) during start-up of the IM
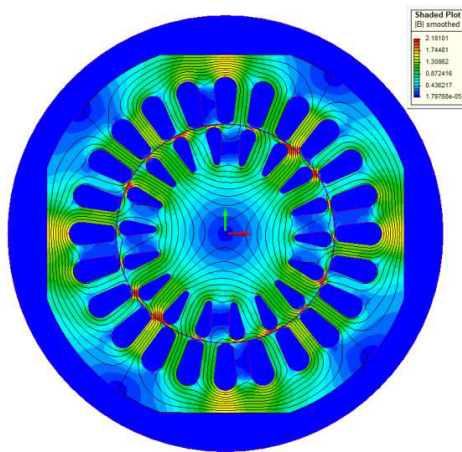

Fig. 4. Distribution of the magnetic flux density
and magnetic field lines at chosen time instant at
the steady state operation of the IM

considered. The developed parameterized numerical models enable the study of the impact of the angular extent α and the depth h of the rotor cut-out on the maximum value of the reluctance torque and on the course of the start-up process. For the LSPMSM, permanent magnets were placed in the rotor cut-out of the S1 rotor structure (Fig. 5(c)) and the influence of their angular extent and height on the obtained synchronous torque was examined. The maximum torque value was determined on the basis of the determined relationship between the electromagnetic torque T and the rotor rotation angle ϑ. It was assumed that for each angular position of the rotor, the stator phase windings are supplied with direct current with values resulting from a given time step. When calculating the values of instantaneous phase currents, it was assumed that the RMS currents I are equal to the rated current I_N of the IM. An example characteristic of the electromagnetic torque T versus the rotor angle ϑ is shown in Fig. 6(a).

In order to determine the values of the angle extent α and the cut-out depth h, for which the highest value of $T_{\max}$ of torque vs. rotor position angle characteristic is obtained, the optimization calculations were carried out for both considered structures of the rotor. Due to the small number
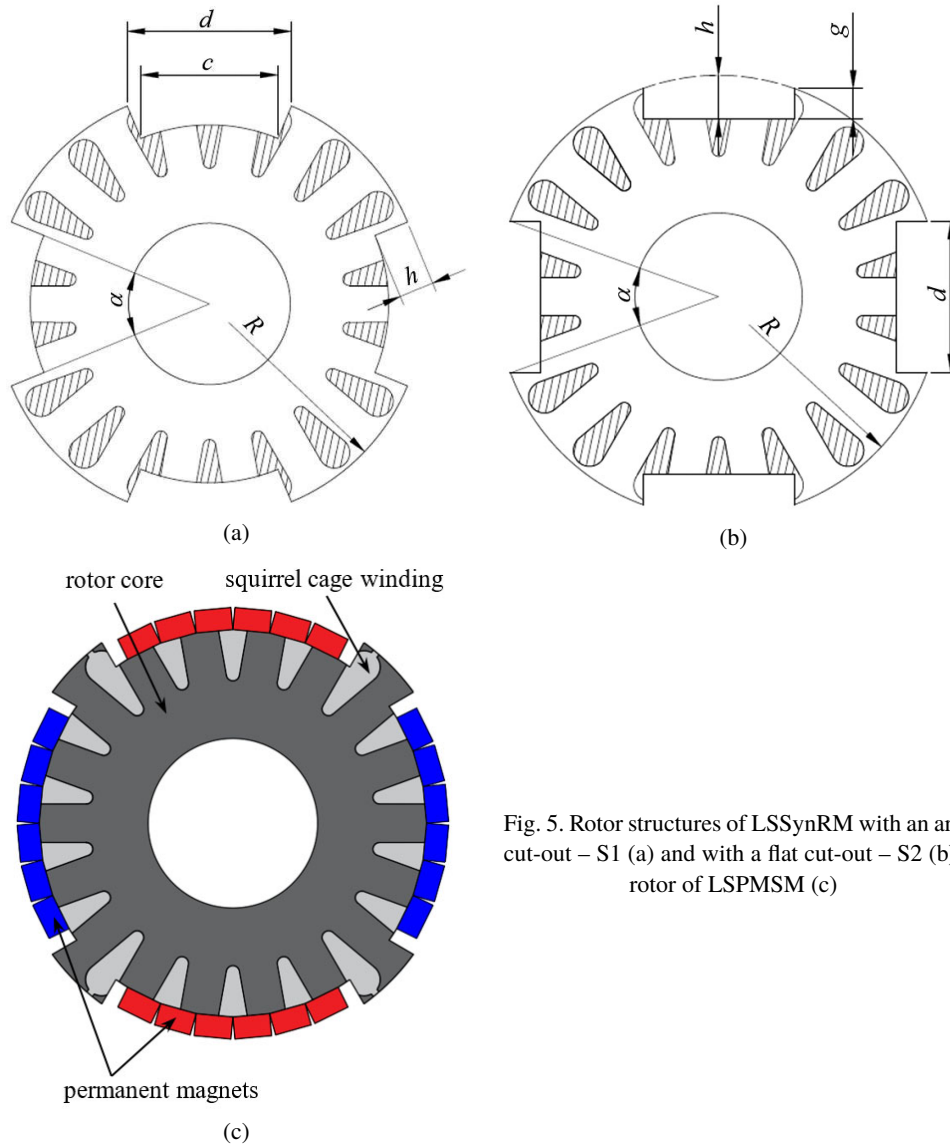
(a)   (b)

Fig. 5. Rotor structures of LSSynRM with an arc cut-out – S1 (a) and with a flat cut-out – S2 (b); rotor of LSPMSM (c)

(c)

of design variables, the systematic review method was used in the optimization process. The obtained dependencies of the maximum torque T_{max} on the angle α for selected values of the parameter h are shown in Fig. 6(b). The optimal values of the parameters α and h for the studied structures have been summarized in Table 1. In the proposed approach, in order to shorten the calculation time, after the time-consuming optimization of the shape of the cut-outs, the analyses of the start-up process have been performed for the rotor variants for which the highest torque performance was obtained. The simulations of the start-up process have been carried out for the load torque $T = 1$ Nm and the load moment of inertia equal to 1.2 of the rotor inertia and
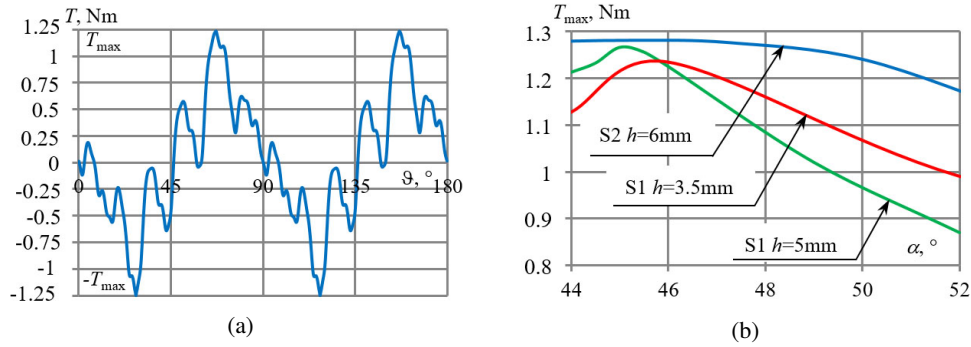
(a)

(b)

Fig. 6. Electromagnetic torque T as a function of rotor rotation angle ϑ for variant S2 at $I = I_N$, $\alpha = 45°$ and $h = 6$ mm (a); maximum torque T_{max} as a function of the cut-out span α for $I = I_N$ and $h = $ const (b)

confirmed the starting capabilities of the designed motors. Exemplary rotational speed waveforms during the LSSynRM start-up with the S1 variant of the rotor structure are shown in Fig. 7. It can be seen that the start-up time is relatively short, after 10 periods of the supply voltage it can be stated that the rotor falls into synchronism. Similar simulations of a motor start-up process were carried out for the LSPMSM. The best functional parameters and shortest start-up time were obtained for magnets with a height of 3 mm and span equal to 65% of the pole pitch. N38 neodymium magnets were used. The optimized dimensions of rotor's cut-outs are summarized in Table 1.

Table 1. Optimized values of design parameters for S1 and S2 rotor variants

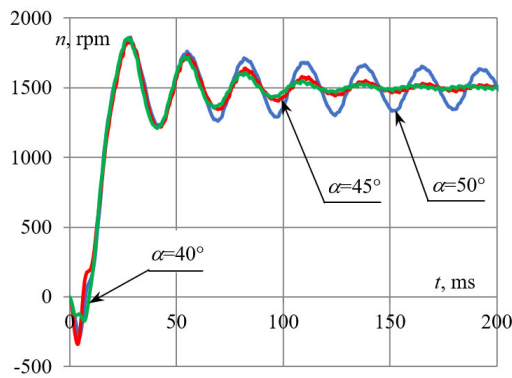| Motor	Rotor	α [°]	h [mm]
LSSynRM	S1	45	6
LSSynRM	S2	45	5
LSPMSM	S1	60	3.5

Fig. 7. Rotational speed waveforms for selected span cut-outs α of S1 rotor at $h = 5$ mm

Exemplary distributions of the magnetic flux density and the magnetic field lines obtained for the optimized rotor designs of structures S2 with flat and S1 with arc cut-outs of both types of the studied motors are shown in Fig. 8.
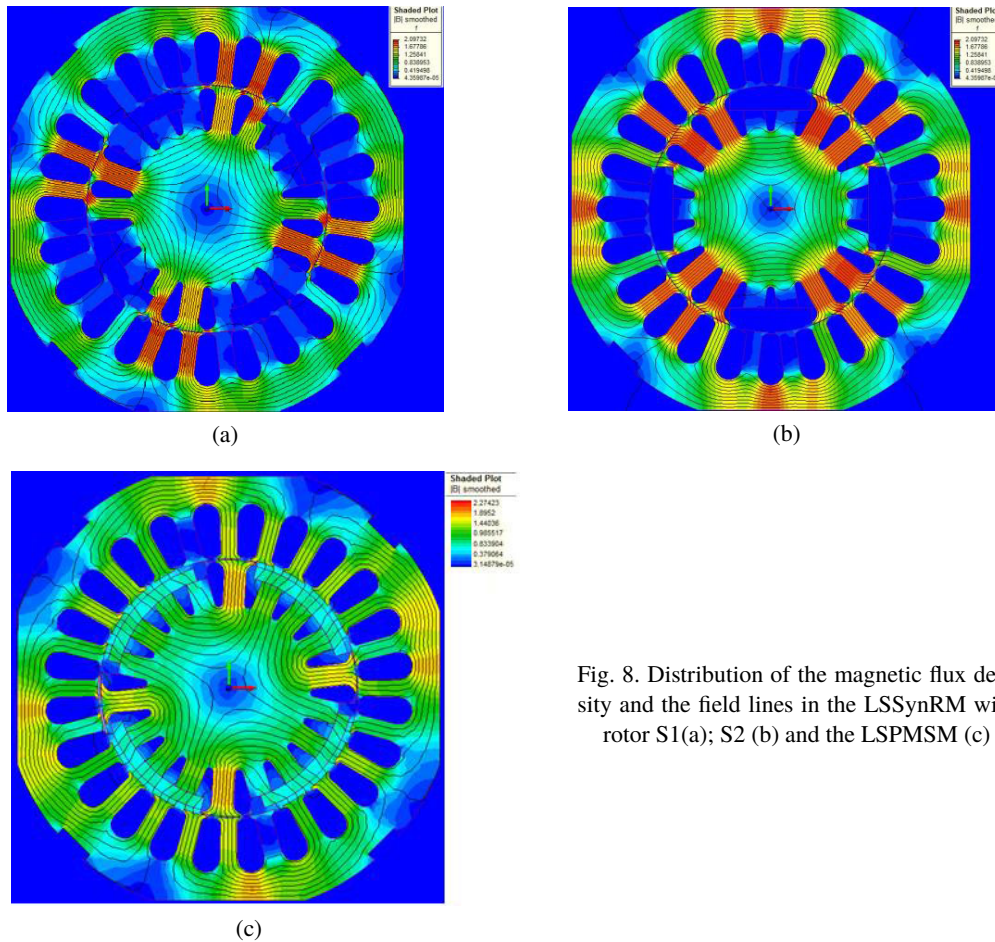

(a)

(b)

(c)

Fig. 8. Distribution of the magnetic flux density and the field lines in the LSSynRM with rotor S1(a); S2 (b) and the LSPMSM (c)

In the next stage of the work, the prototypes of the S2 rotor for the LSSynRM and S1 rotor for the LSPMSM with optimal cut-out dimensions were fabricated. Then, experimental tests of the developed prototype motors were carried out and compared with the results of the IM's performance. It should be emphasized that in all the tested motors the same core and stator winding were used as in the mass-produced Sh71-4A motor.

3. Experimental tests of studied motors

The IM, as well as designed and fabricated prototypes of the LSSynRM and the LSPMSM, were tested on a specially designed and developed measuring stand (Fig. 9). It was found that at

the rated phase voltage of the IM (equal to 230 V for the stator phase windings arranged into a star connection) both developed prototypes draw a much higher value of the phase current than the IM. The main reason of the increased value of current at the rated voltage is the decreased equivalent permeance of the air-gap due to imposed cut-outs in the rotor structure and the strong saturation of the non-silent poles. As the proposed design method at the current state does not include the modification of the stator winding to fit the grid voltage level, the tests were carried out at a reduced value of the supply voltage.
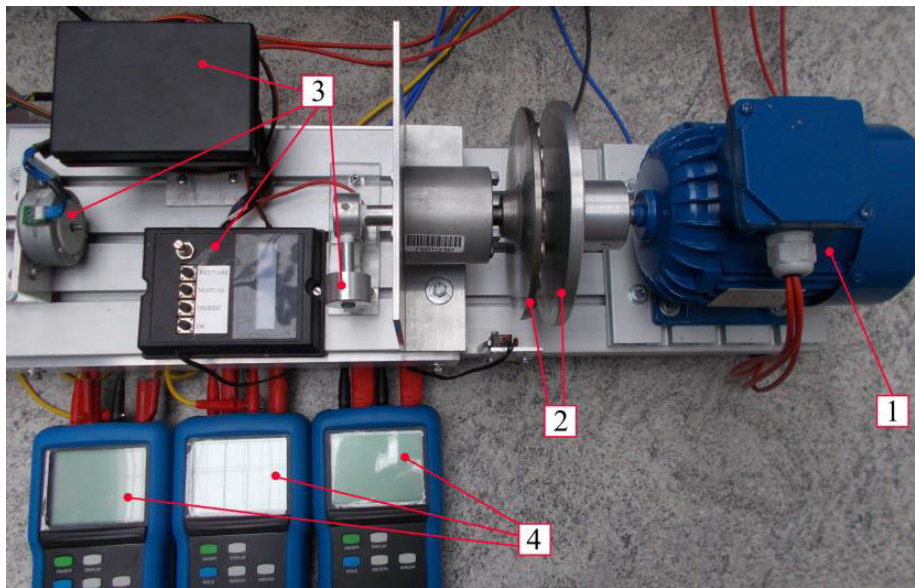

Fig. 9. Test bench: 1 – tested motor, 2 – PM eddy-current brake, 3 – torque setting and measurement system, 4 – voltage, current and power measurement system

The measurements were carried out at different values of the supply voltage and for such a range of load torques for which the phase current did not exceed the rated value I_N. Based on the results of the measurements, the characteristics of the efficiency and the power factor for all three tested motors were determined (Fig. 10). The values of the efficiency and the power factor for the selected supply voltages and the rated value of the phase current I_N have been summarized in Table 2.

The analysis of the obtained results of the IM's, LSSynRM's and LSPMSM's performance shows that at the I_N current the LSSynRM provides less power (less torque) than the IM. However, at lower voltages (180 V and 160 V) this motor has similar efficiency as the IM, and the power factor is about 27% lower than in the IM. Also, the power on the shaft drops about 25% comparing to the IM power. The LSPMSM has a very high power factor and much better efficiency than the IM. The embodied energy efficiency factor defined as the efficiency and power factor product ($\eta \cos \varphi$) of the LSPMSM is about 34% higher than that of the IM. Lowering the supply voltage increases the power factor and reduces the efficiency of the motors. The LSSynRM achieved even higher efficiency than the IM at 160 V and 180 V (Table 2). The load torque at which the rated

current flows in the stator windings also decreases. In order to adapt the motor to supply from a 400 V standard three-phase grid, a stator winding of the LSSynRM and the LSPMSM should be redesigned and rewound.

The influence of the supply voltage at constant load torque on the energy performance of the tested motors was also examined. The obtained results for the selected load torque equal to half
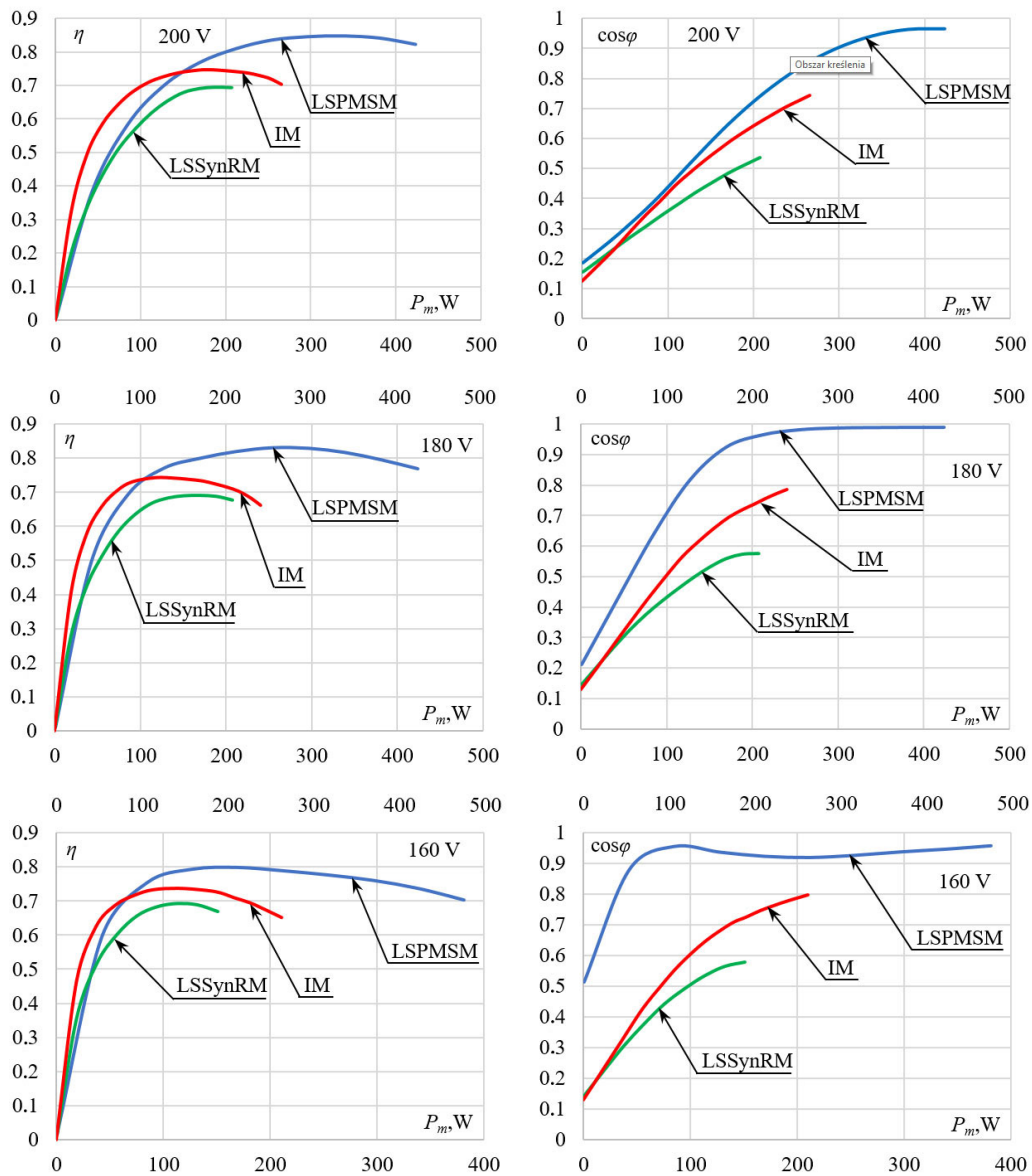

Fig. 10. Efficiency η and power factor $\cos\varphi$ as a function of power on the shaft of three motors IM, LSSynRM, LSPMSM for three selected phase supply voltages

Table 2. Efficiency η and power factor $\cos\varphi$ for the rated current I_N for studied machines

Motor	200 V		180 V		160 V	
	$\cos\varphi$	η	$\cos\varphi$	η	$\cos\varphi$	η
IM	0.744	0.702	0.785	0.661	0.798	0.649
LSSynRM	0.512	0.695	0.573	0.687	0.582	0.665
LSPMSM	0.964	0.831	0.987	0.809	0.937	0.761

the rated torque of the IM ($T = 0.5T_N$) are shown in Fig. 11. The best energy performance of the LSPMSM and the LSSynRM is obtained at supply voltage equal to approx. 170 V and 160 V, respectively. Increasing the load torque value results in higher values of the efficiency and the power factor for the studied motors at higher supply voltages. This is confirmed by the results presented in Fig. 11.
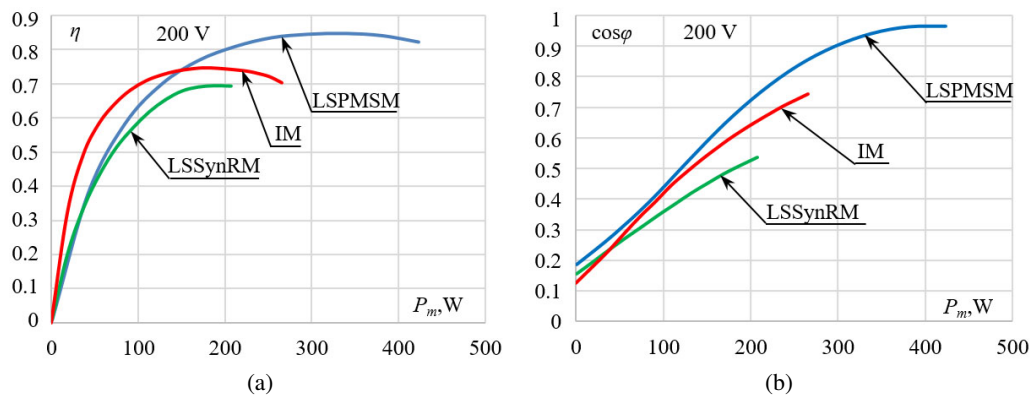

Fig. 11. Efficiency η and power factor $\cos\varphi$ as a function the phase supply voltage of the IM, LSSynRM, LSPMSM at load torque $T = 0.5T_N$

4. Conclusions

The study presented in the paper discusses low-cost prototypes of an LSSynRM and LSPMSM that were developed on the basis of a general-purpose asynchronous squirrel cage motor of the Sh71-4A type. For this purpose, a squirrel cage rotor was optimized to obtain the best functional parameters characterizing the steady state operation of both line-start synchronous motors, while meeting the additional requirements for providing the asynchronous start-up. Field-circuit models were developed to perform the design and optimization calculations. The field-circuit models of electromagnetic phenomena in the studied LSSynRM and LSPMSM were elaborated and exploited during the optimization process. The numerical models and design calculations have been performed using a professional FEM package, MagNet. The developed models were based on the validated IM model elaborated within the previous research. The proposed approach

ensures the reliability of the simulation results. Detailed conclusions regarding the results of the performed experimental tests on these motors are given and discussed in section 3 of this paper.

The presented tests show that based on the components of mass-produced IMs, low cost synchronous motors with good energy performance can be implemented in production. These motors can be used in drives with constant rotational speed as an alternative to classical squirrel cage induction motor drives. Based on the comparative analysis of the tested motors under a wide range of load torque changes, it can be concluded that the energy performance of the LSSynRM is slightly worse than that of the IM. However, it should be noted that the LSSynRM, at the low values of the load torques and using rewound stator, it is possible to achieve similar efficiency to that of the IM. The LSPMSM has much better energy parameters ($\cos \varphi$, η) than the IM and the LSSynRM. In addition, the designed LSPMSM provides higher power than the IM and the LSSynRM without exceeding the rated value of the phase current. It is therefore advisable to carry out further intensive design and optimization work on the development of line-start capable synchronous motors that helps to improve their energy performance.

References

[1] Zawilak T., *Influence of rotor's cage resistance on demagnetization process in the line start permanent magnet synchronous motor*, Archives of Electrical Engineering, vol. 69, no. 2, pp. 249–258 (2020), DOI: 10.24425/aee.2020.133023.

[2] Jędryczka C., Knypiński Ł., Demenko A., Sykulski J.K., *Methodology for cage shape optimization of a permanent magnet synchronous motor under line start conditions*, IEEE Transactions on Magnetics, vol. 54, no. 3, pp. 1–4 (2018), DOI: 10.1109/TMAG.2017.2764680.

[3] Zawilak J., Gwoździewicz M., *Start-up of large power electric motors with high load torque*, Electrical Review, vol. 95, no. 6, pp. 145–148 (2019), DOI: 10.15199/48.2019.06.27.

[4] Wymeersch B., Belie F., Rasmussen C., Vandevelde L., *Classification method to define synchronization capability limits of line start permanent magnet motor using mesh-based magnetic equivalent circuit computation results*, Energies, vol. 11, no. 4, pp. 1–22 (2018), DOI: 10.3390/en11040998.

[5] Baranski M., Szelag W., Lyskawinski W., *An analysis of a start-up process in LSPMSMs with aluminum and copper rotor bars considering the coupling of electromagnetic and thermal phenomena*, Archives of Electrical Engineering, vol. 68, no. 4, pp. 933–946 (2019), DOI: 10.24425/aee.2019.130693.

[6] Rabbi S., Rahman M.A., *Critical criteria for successful synchronization of line-start IPM motor*, IEEE Journal of Emerging and Selected Topics Power Electronics, vol. 2, pp. 348–358 (2014), DOI: 10.1109/JESTPE.2013.2295178.

[7] Takahashi A., Kikuchi S., Miyata K., Binder A., *Asynchronous torque of line-starting permanent-magnet synchronous motors*, IEEE Transactions on Energy Conversion, vol. 30, no. 2, pp. 498–506 (2015), DOI: 10.1109/TEC.2014.2361836.

[8] Baranski M., Szelag W., Jedryczka C., *Influence of temperature on partial demagnetization of the permanent magnets during starting process of line start permanent magnet synchronous motor*, International Symposium on Electrical Machines (SME), on-line: IEEE Xplore, pp. 1–6 (2017), DOI: 10.1109/ISEM.2017.7993535.

[9] Nishiyama N., Uemura H., Honda Y., *Highly Demagnetization Performance IPMSM Under Hot Environments*, IEEE Transactions on Industry Applications, vol. 55, no. 1, pp. 265–272 (2019), DOI: 10.1109/TIA.2018.2863666.

[10] Sjökvist S., Eriksson S., *Investigation of Permanent Magnet Demagnetization in Synchronous Machines during Multiple Short-Circuit Fault Conditions*, Energies, vol. 10, no. 10, p. 1638 (2017), DOI: 10.3390/en10101638.

[11] Bavendiek G., Müller F., Sabirov J., Hameyer K., *Magnetization dependent demagnetization characteristic of rare-earth permanent magnets*, Archives of Electrical Engineering, vol. 69, no. 1, pp. 33–45 (2019), DOI: 10.24425/AEE.2019.125978.

[12] Ruoho S., Kolehmainen J., Ikaheimo J., Arkkio A., *Interdependence of Demagnetization, Loading, and Temperature Rise in a Permanent-Magnet Synchronous Motor*, IEEE Transactions on Magnetics, vol. 46, no. 3, pp. 949–953 (2010), DOI: 10.1109/TMAG.2009.2033592.

[13] Kim W.H., Kim K.S., Kim S.J., Kang D.W., Go S.C., Chun Y.D., Lee J., *Optimal PM design of PMA-SynRM for wide constant-power operation and torque ripple reduction*, IEEE Transactions on Magnetics, vol.45, no. 10, pp. 4660–4663 (2009).

[14] Abramenko V., Petrov I., Pyrhönen J., *Analysis of damper winding designs for direct-on-line synchronous reluctance motor*, 43rd Annual Conference of the IEEE Industrial Electronics Society (IECON 2017), on-line: IEEE Xplore, pp. 1802–1809 (2017), DOI: 10.1109/IECON.2017.8216305.

[15] Aguba V., Muteba M., Nicolae D.V., *Transient analysis of a start-up synchronous reluctance motor with symmetrical distributed rotor cage bars*, AFRICON 2017, on-line: IEEE Xplore, pp. 1290–1295 (2017), DOI: 10.1109/AFRCON.2017.8095668.

[16] Gamba M., Armando E., Pellegrino G., Vagati A., Janjic B., Schaab J., *Line-start synchronous reluctance motors: Design guidelines and testing via active inertia emulation*, Energy Conversion Congress and Exposition (ECCE2015), on-line: IEEE Xplore, pp. 4820–4827 (2015), DOI: 10.1109/ECCE.2015.7310340.

[17] Kolehmainen J., *Synchronous reluctance motor with form blocked rotor*, IEEE Transactions on Energy Conversion, vol. 25, no. 2, pp. 450–456 (2010).

[18] Tang K., Zhou L., Wang J., Xiao Y., Wang S., *Rotor design and optimization of the single-phase line-start synchronous reluctance motor*, 20th International Conference on Electrical Machines and Systems (ICEMS), on-line: IEEE Xplore, pp. 1–4 (2017), DOI: 10.1109/ICEMS.2017.8056082.

[19] Ershad N.F., Mirsalim M., Aliabad A.D., *Line-start permanent magnet motors: Proper design for pole-changing starting method*, IET Electric Power Applications, vol. 7, no. 6, pp. 470–476 (2013), DOI: 10.1049/iet-epa.2012.0059.

[20] Jedryczka C., Wojciechowski R.M., Demenko A., *Finite element analysis of the asynchronous torque in LSPMSM with non-symmetrical squirrel cage winding*, International Journal Applied of Electromagnetics and Mechics, vol. 46, no. 2, pp. 367–373 (2014), DOI: 10.3233/JAE-141947.

[21] Knypiński Ł., Pawełoszek K., Le Menach Y., *Optimization of Low-Power Line-Start PM Motor Using Gray Wolf Metaheuristic Algorithm*, Energies, vol. 13, no. 5, pp. 1186-1–1186-11 (2020), DOI: 10.3390/en13051186.

[22] Sarani E., Vaez-Zadeh S., *Design procedure and optimal guidelines for overall enhancement of steady-state and transient performances of line start permanent magnet motors*, IEEE Transactions on Energy Conversion, vol. 32, no. 3, pp. 885–894 (2017), DOI: 0.1109/TEC.2017.2694485.

[23] Fei W., Luk P.C.K., Ma J., Shen X.J., Yang G., *A High-Performance Line-Start Permanent Magnet Synchronous Motor Amended From a Small Industrial Three-Phase Induction Motor*, IEEE Transactions on Magnetics, vol. 45, no. 10, pp. 4724–4727 (2009), DOI: 10.1109/TMAG.2009.2022179.

[24] Kazumi Kurihara M., Rahman A., *High-efficiency line-start interior permanent magnet synchronous motors*, IEEE Transactions on Industry Applications, vol. 40, no. 3, pp. 789–796 (2004), DOI: 10.1109/TIA.2004.827476.

[25] Melfi M.J., Umans S.D., Atem J.E., *Viability of highly efficient multi-horsepower line-start permanent-magnet motors*, IEEE Transactions on Industry Applications, vol. 51, no. 1, pp. 120–128 (2014), DOI: 10.1109/TIA.2014.2347239.

[26] Krings A., Boglietti A., Cavagnino A., Sprague S., *Soft Magnetic Material Status and Trends in Electric Machines*, IEEE Transactions on Industrial Electronics, vol. 64, no. 3, pp. 2405–2414 (2017), DOI: 10.1109/TIE.2016.2613844.

[27] Łyskawiński W., Jędryczka C., Szeląg W., *Influence of magnet and cage shape on properties of the line start synchronous motor with powder hybrid rotor*, International Symposium on Electrical Machines (SME 2017), pp. 1–6 (2017), DOI: 10.1109/ISEM.2017.7993556.

[28] Ślusarek B., Kapelski D., Antal L., Zalas P., Gwoździewicz M., *Synchronous motor with hybrid permanent magnets on the rotor*, Sensors 2014, vol. 14, no. 7, pp. 12425–12436 (2014), DOI: 10.3390/s140712425.

[29] Baranski M., *FE analysis of coupled electromagnetic-thermal phenomena in the squirrel cage motor working at high ambient temperature*, COMPEL – International Journal for Computation and Mathematics in Electrical and Electronic Engineering, vol. 38, no. 4, pp. 1120–1132 (2019), DOI: 10.1108/COMPEL-10-2018-0384.

[30] Pałka R., Woronowicz K., Kotwas J., Xing W., Chen H., *Influence of different supply modes on the performance of linear induction motors*, Archives of Electrical Engineering, vol. 68, no. 3, pp. 473–483 (2019), DOI: 10.24425/aee.2019.129335.

[31] Knypiński Ł., Jędryczka C., Demenko A., *Influence of the shape of squirrel-cage bars on the dimensions of permanent magnets in an optimized line-start permanent magnet synchronous motor*, Electrical and Electronic Engineering, vol. 36, no. 1, pp. 298–308 (2017), DOI: 10.1108/COMPEL-03-2016-0103.